CrystEngComm

Accepted Manuscript

ROYAL SOCIETY OF CHEMISTRY

www.rsc.org/crystengcomm

Dynamic Article Links ►

Cite this: DOI: 10.1039/c0xx00000x

www.rsc.org/xxxxxx

ARTICLE TYPE

Lanthanide Contraction Effects on Structures, Thermostabilities, and CO_2 Adsorption and Separation Behaviors of Isostructural Lanthanide-Organic Frameworks

Weijun Mu,[1] Xin Huang,[2] Ruiqin Zhong,[2] Wei Xia,[1] Jia Liu,[1] Ruqiang Zou[1],*

Received (in XXX, XXX) Xth XXXXXXXXX 20XX, Accepted Xth XXXXXXXXX 20XX
DOI: 10.1039/b000000x

A systematic investigation of CO_2 adsorption and separation behaviours toward fourteen isostructural lanthanide-organic frameworks (LOFs) of lanthanide benzenetricarboxylate (LnBTC) is executed, where Ln = Y, La, Ce, Pr, Nd, Sm, Eu, Gd, Tb, Dy, Ho, Er, Tm and Yb. These LOFs are facilely synthesized and randomly scaled by heating the mixture of 1,3,5-benzenetricarboxylic acid and lanthanide nitrate solution with reaction time less than 1 h. Structure refinement reveals these LOFs exhibit three-dimensional networks with one-dimensional channels and open metal sites on the pore walls. Thermogravimetric analyses verify that these LOFs can firmly stabilize up to 540 °C. Influenced by the opposite effect of ionic radius and molecular mass from Y(III)-Yb(III), the related LOFs with highest CO_2 uptakes of YBTC at 273 K and PrBTC at 298 K in atmosphere pressure, respectively. Moreover, the real CO_2 separation from binary gas mixtures of CO_2/N_2 and CO_2/CH_4 further convince that lanthanide contraction act as the important roles to tune the adsorption and separation performance of the resulting materials. This work may give rise to a potential application perspective of highly thermostable porous LOF materials for carbon dioxide capture from flue gas and natural gas to reduce the greenhouse emissions and improve energy efficiency.

Introduction

Carbon dioxide (CO_2) is the primary greenhouse gas emitted through the combustion of fossil fuels such as oil, coal and natural gas. CO_2 separation, capture and sequestration is a set of technologies that can potentially reduce CO_2 emissions from power plants, industrial processes, and other stationary sources of CO_2.[1,2] Due to its economic advantage and environmentally friendly nature, separation technologies using physical adsorption demonstrates promising and attractive applications compared to other CO_2 separation technologies such as chemical absorption, membrane filtration and cryogenic separation.[3] The adsorption capacity and selectivity are the two most important evaluation indexes of adsorbents.[4,5] Porous materials with intensive pore structures ensure that they have excellent adsorption ability as adsorbents.

Emerging as a new class of porous materials in the past two decades, metal-organic frameworks (MOFs) consisting of organic linker and metal nodes have been widely investigated for adsorption-based CO_2 separation in virtue of their high surface area, tunable pore size and functional pore walls.[6-10] Up to now, various strategies are employed to improve CO_2 adsorption and separation performances within MOF materials including: tuning of pore size contribution,[9,11,12] functionalization of pore walls,[13-17] utilization of the vacancy of Lewis acid sites[18-20] and so on.[21-28]

On the other hand, most MOFs have relative lower thermostability than other porous materials such as zeolites, porous carbon, etc., which will directly affect their industrial application. For example, copper(II) bezenetricarboxylate, namely HKUST-1, can only be stable up to 300 °C in nitrogen atmosphere,[29] and thus restricts their real industrial application. Therefore, MOFs with high themostability are of practical value. Various functionalization methods are available to introduce different metal centers to MOFs to improve their thermostability.[30,31] As a new family of MOFs, Lanthanide-organic frameworks (LOFs) with lanthanides as metal nodes are exactly such porous materials with the desirable property for their potential applications in optical, electronic, sensing, gas separation and catalytic area.[32-38] Recently, several lanthanide benzenetricarboxylate (LnBTC) have been investigated as promising candidate for gas storage and separation.[34,39-45] However, almost all of the reports focused on one or several certain lanthanide LOFs and there is still a lack of systematic study on series of LOFs for CO_2 separation. Although considerable investigation has been made towards LOFs gas adsorption properties,[31,39,41,46-53] it is also necessary to prepare LOFs in large scale for the potential industrial application.

Of great interest in this paper is to massively and quickly prepare fourteen highly thermostable and isostructural LOFs of LnBTC. These LnBTC are synthesized by simple heat treatment of 1,3,5-benzenetricarboxylic acid (H_3BTC) and lanthanide nitrate solution less than 1 h, where Ln = Y, La, Ce, Pr, Nd, Sm, Eu, Gd, Tb, Dy, Ho, Er, Tm and Yb. Powder X-ray diffraction

(PXRD) refinement and thermogravimetric analysis (TGA) are performed to investigate the lanthanide contraction effects induced structural and thermostable discrepancy. Furthermore, the static and dynamic CO_2 separation experiments from CO_2/CH_4, CO_2/N_2 mixtures are carried out to provide information on the adsorption selectivity which affects the subsequent separation efficiency.

2. Materials and methods

All solvents and reagents for synthesis are commercially available and used as received without further purification.

2.1 Sample preparation

All LOFs have been synthesized by the same procedures. The only difference lies in the various lanthanide salts. Therefore, YBTC is selected as an example. The synthesis of YBTC is carried out by the addition of $Y(NO_3)_3{\cdot}6H_2O$ (3.677g, 9.6 mmol) and H_3BTC (1.681g, 8 mmol) to the solvent of N,N’-dimethylformamide (DMF, 50 mL) and deionized water (10 mL) in a volumetric flask at room temperature. Triethylamine (0.4 mL) and nitric acid (0.2 mL) are added and the reaction is allowed to proceed with magnetic stirring for less than 1h at 110 °C. The resulted LOFs are purified by washing with ethanol for three times and dried at room temperature in a vacuum oven to obtain the desired product. This reaction can be scaled up to 10 to 20 times of starting materials without compromising the yield. Similar procedure are employed to synthesize other LOFs by replacing $Y(NO_3)_3{\cdot}6H_2O$ with the same molar amount of $Ln(NO_3)_3{\cdot}xH_2O$, where Ln = La, Ce, Pr, Nd, Sm, Eu, Gd, Tb, Dy, Ho, Er, Tm and Yb. The reaction schemes are shown in Scheme 1 and Fig. S1 (Supporting Information). PXRD analysis shows that the products from the reaction within 1h has the same phase to the one after the 17 h reaction (Fig. S2).

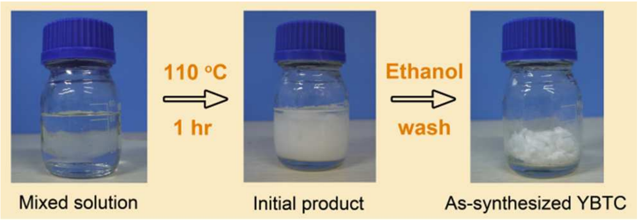

Scheme 1 Schematic illustration of synthesis of YBTC.

2.2 Thermogravimetric analyses

TGA experiment is carried out by using a SDT Q600 from TA instrument. The decomposition measurements based on TGA are conducted between room temperature and 750 °C at a scanning rate of 5 °C/min under nitrogen atmosphere (100 mL/min). The sample weight is approximately 5 mg for all the experiments.

2.3 Powder X-ray diffraction

PXRD data is collected at ambient atmosphere and temperature on Rigaku Dmax/2400 X-ray diffractometer operated at 40 kV and 100 mA using Cu Kα radiation. The profile-fitting and Reitveld refinements of LnBTC samples are performed by using program TOPAS 2.1,[54] adopting the previously known cell parameters and atomic positions of NdBTC[53] as initial structure model.

2.4 Gas adsorption

Gas adsorption measurements are performed by a Quantachrome Autosob iQ adsorption analyzer. The raw samples are activated under dynamic vacuum with no more than 0.003 mmHg with a heating rate of 5 °C/min. The N_2 sorption isotherms are recorded under pressure from 0.0001 to 0.995 P/P_0 in a liquid nitrogen bath. The gas adsorption experiments of CO_2, CH_4 and N_2 at 273 K and 298 K are carried out in a thermostatic glycol/water bath system.

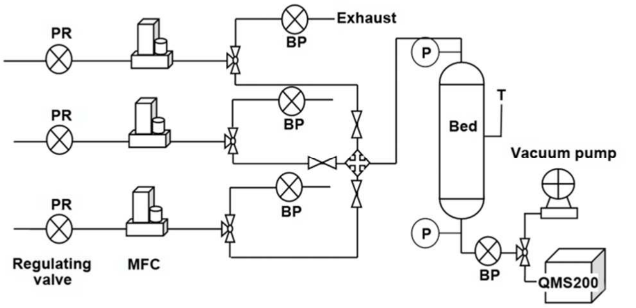

Fig. 1 Schematic diagram of the setup to collect breakthrough curves. PR: pressure regulator; MFC: mass flow controller; BP: back pressure regulator; P: pressure transducer; T: T-type thermocouple; QMS: quadrapole mass spectrograph.

2.5 Breakthrough experiments

The breakthrough experiments apparatus are a home-made setup shown schematically in Fig. 1. The adsorbents are packed in a stainless steel tube of length 80 mm and inner diameter 4 mm. Mass flow controllers of precision ±1% (purchased from Beijing Sevenstar electronics Co. Ltd.) are used to control the flow rates in the passages of the absorber. A back-pressure regulator is used to control the pressure over the adsorption bed and a pressure transducer with accuracy ±0.1% is used to detect the pressure. Pressure at both entrance and exit of the adsorption bed is detected, and the pressure drop over the bed is thus obtained. All parts are connected with stainless steel capillary tubes of inner diameter 2 mm and wall thickness 0.5 mm. The test temperature is kept constant within ±0.10 °C by using a thermostat. The outlet gases are detected by using a QMS 200 mass spectrometer with a sampled rate of 1 point per second. The concentration of the outlet gas is calibrated by comparing it to the concentration of the source gas recorded by the mass spectrometer under the same flow rate.

3. Result and discussion

3.1 Structure

Crystal structures of LnBTC have been previously reported by using single crystal XRD determination except for TmBTC.[34,48-50] These LOFs consist of BTC ligands coordinated to lanthanide ions in 1:1 stoichiometric ratio. As shown in Fig. 2, the adjacent lanthanide ions are bridged by μ_2 carboxylate groups to assemble into a one-dimensional (1D) helix metal chain. Furthermore, their structures contain 1D channel and open metal active sites.[53]

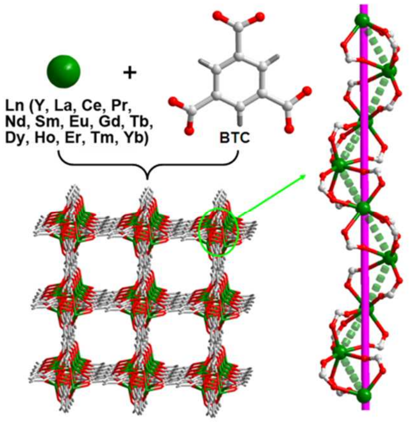

Fig. 2 Crystal structures of LnBTC with 1D channel and open metal sites.

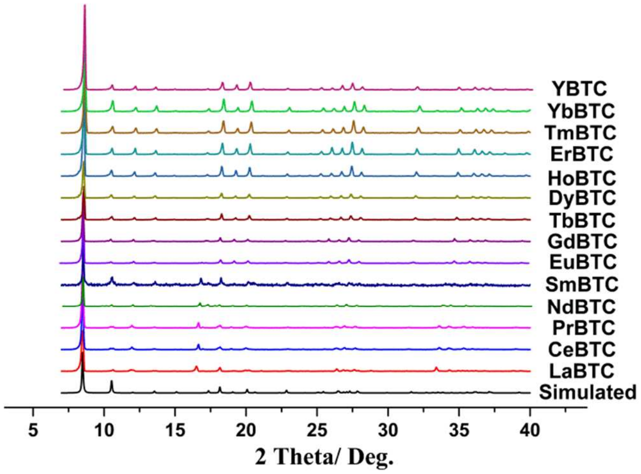

Fig. 3 PXRD patterns of LnBTC.

Verified by the PXRD patterns, LnBTC synthesized in this work have consistent structure as the previously reported ones.[53] They all demonstrate good crystallinity and purity (Fig. 3). PXRD refinements are carried out to investigate the difference of unit cell parameters (Fig. 4). As is well known, the Ln(III) ions exhibit inherent lanthanide contraction with radii ranged from 103 to 87 pm (Table S1). The *a*- (and *b*-) parameters of LnBTC decrease gradually with decreasing ionic radius of the Ln(III) ion except for LaBTC and YBTC, which in turn decrease with increasing atomic number.[53] The corresponding parameter of LaBTC falls in between SmBTC and EuBTC, and YBTC is similar to that of ErBTC. However, the *c*-parameter lacks any obvious trend, in which CeBTC and SmBTC represent two endpoint of maximum and minimum. Affected by *a*- and *b*-parameters, the unit cell volumes of LnBTC show the overall decreasing trend, in which LaBTC, SmBTC and YBTC deviate from this trend. Therefore, lathanide contraction effects act as the important role to tune the lattice parameter along with *a* and *b* axis and unit cell volume of LnBTC.

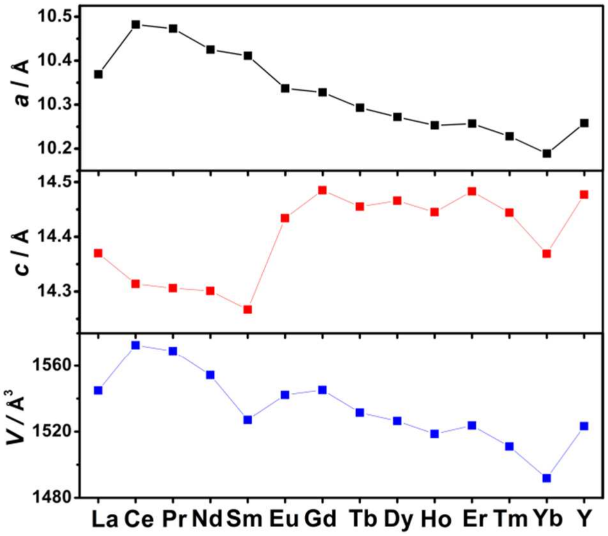

Fig. 4 Unit cell parameter a (Å), c (Å) and V (Å³) of LnBTC as obtained from PXRD refinement, compared with the ionic radii of Lanthanide ions.

3.2 Thermal behaviour

TGA experiments are conducted to determine the thermal stabilities of these isostructural LOFs, which is important for MOF materials application.[55] As shown in Fig. 5a, the host frameworks of LnBTC are firmly stable up to 540 ℃ and the one-step weight loss rapidly happens from 540 to 660 ℃, indicating the decomposition of the target compounds. It is very interesting that these LOFs pass through quite different desolventized process (Fig. 5b). It can be easily divided these LOFs into two families with increasing atomic number except for YBTC according to TGA curves. The removals of all free and coordinated solvents of La- to EuBTC go through three steps up to 420 ℃ under nitrogen atmosphere. Gd- to YbBTC and YBTC show only two steps for desolventization. These LOFs are comparable to those MOFs with the highest thermal stabilities.[56-58] Instead, these coordinated solvents within LOFs can be removed less than 350 °C under vacuum in replacement of flowing nitrogen atmosphere without decomposition of their host frameworks. The TGA curve of activated YBTC after treated at 340 °C under vacuum for 6 h shows there is almost no more weight loss until 540 °C (Fig. S3). In general, degradation of the organic components of MOFs typically begins at moderate temperatures (200-350 ℃), resulting in decomposition of the synthesized materials. In this regards, LOFs exhibit excellent thermal stabilities due to their high coordination number and strong bonding interactions of Ln-O bonds. Therefore, the as-synthesized samples of LnBTC are thermally treated at 350 °C in vacuum for 6 h to achieve activated samples for characterization and properties measurements, such as gas adsorption and separation experiments.

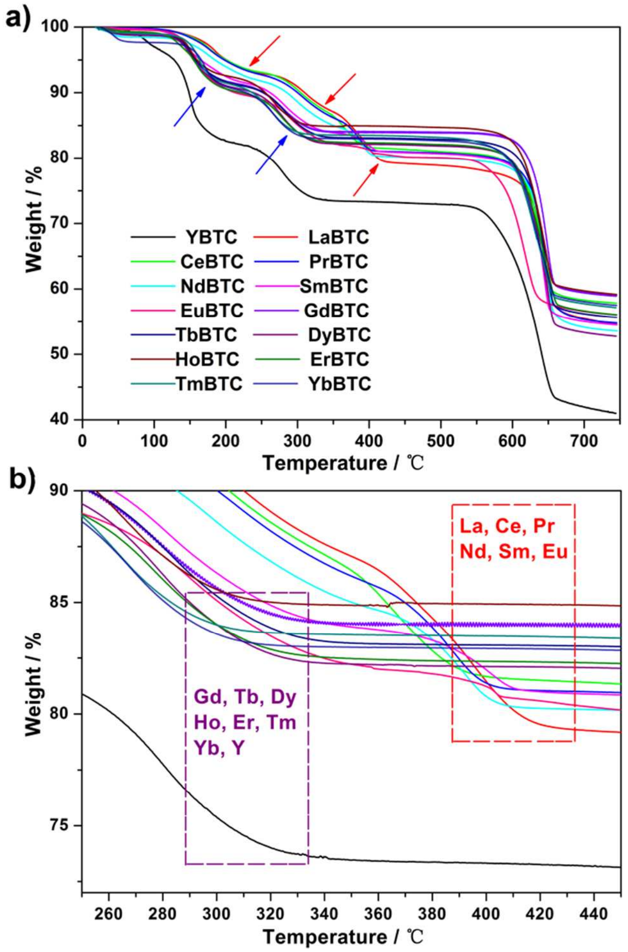

Fig. 5 TGA curves of LnBTC: (a) from room temperature to 750 °C. The blue and red arrows represent various desolventized steps, and (b) the enlarged view of the desolventized curves. The purple and red dash boxes represent two families of LnBTC.

3.3 Gas adsorption

Gas sorption properties of N_2, CH_4 and CO_2 are investigated for all LnBTC samples. Before the sorption measurements are performed, the as-synthesized products are activated at 350 ºC for 6 h in vacuum to remove the free and coordinate solvent molecules. The solvent-free samples have coordinately unsaturated metal centres as active sites for gas adsorption. The surface area of the material is measured by N_2 adsorption at 77 K (Fig. 6a). Table S2 shows their BET and Langmuir surface area calculated according to N_2 sorption isotherms, pore volume, and pore size distribution (Supporting Information). According to the adsorption results, these LnBTC exhibit classical type I adsorption curves with almost no hysteresis, implying permanent porosity. Their BET surface area fall into 740 to 1018 m^2/g, which is comparable to those reported LOFs.[42,50] Take the radius of Ln(III) as the X-axis and surface area (BET and Langmuir) as the Y-axis to investigate the relationship between different lanthanide ions and the surface area (Fig. 6b). We find that the surface area of the related LOFs has no positive linear relationship with the increase of radius. YBTC has the highest surface area due to its lowest molecular mass and the relative small ionic radius (90 pm) of Y(III) ions. The pore size distributions of LnBTC are calculated by the NLDFT method. The results show that these LOFs are all micropores with the pore sizes falling into 1.1 to 1.5 nm and pore volume of 0.29 to 0.42 cm^3/g.

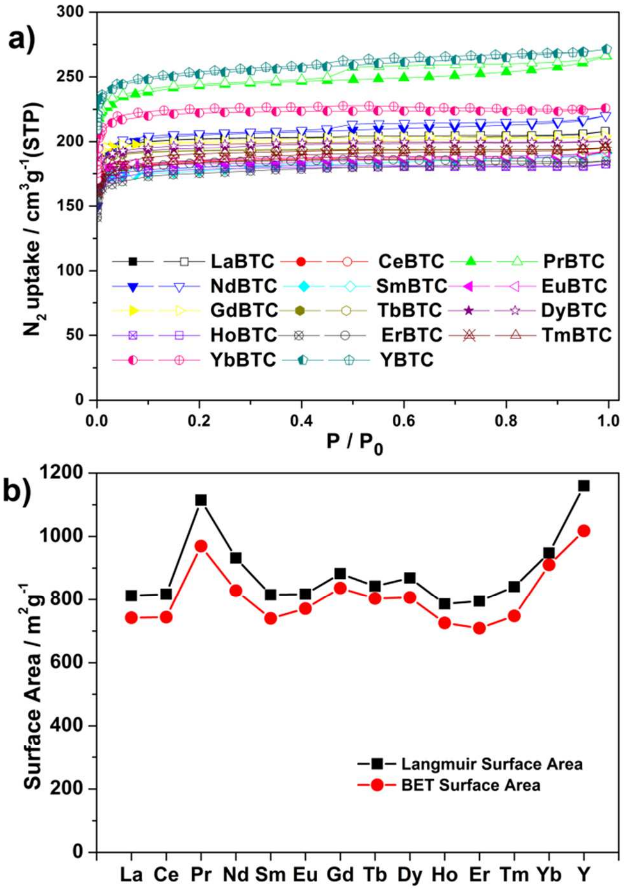

Fig. 6 View of (a) N_2 sorption isotherms of LnBTC at 77K and (b) Langmiur and BET surface area compared with the ionic radii of Lanthanide ions.

Carbon dioxide capture from flue gas or nature gas can not only reduce greenhouse gas emissions but improve energy efficiency. Based on this application background, we carry out CO_2, CH_4 and N_2 sorption experiment of LnBTC. Fig. 7a,b show their sorption isotherms by using static saturated adsorption methods at 273 K and 298 K, respectively. The detailed isotherm for each LOFs is summarized in Figs. S4 to S17 (Supporting Information). YBTC exhibits the largest CO_2 uptake (5.25 mmol/g) among all the samples at 273 K due to its lightest molecular mass (Fig. 7c). However, the largest CO_2 adsorption amount happens to be that of PrBTC (3.02 mmol/g) at 298 K (Fig. 7d). This result indicates that PrBTC shows stronger interactions with CO_2 than that of YBTC.

Furthermore, the isosteric heat Q_{st} of CO_2 adsorption is calculated from isotherm data at 273K and 298K using Clausius−Clapeyron equation:[59]

$$\ln\left(P/[P_0]\right)_n = \frac{Q_{st}}{R}\frac{1}{T} + C$$

Where P and T are the pressure and temperature at the equilibrium state, respectively; $[P_0]$ is the unit of pressure P and n

is the adsorption capacity of corresponding pressure *P* and *T*; *R* and *C* is constant. The calculated CO_2 Q_{st} of LnBTC is shown in Fig. S18. Although the adsorption enthalpy at initial loading varies greatly, less difference on Q_{st} is observed with increasing CO_2 adsorption capacity ranging from 23.0 (GdBTC) to 26.7 kJ/mol (EuBTC). As shown in Fig. S18, The isosteric heats of LnBTC except for the first plots of CeBTC and SmBTC go through an overall increasing trend with increasing CO_2 loading amount. This is attributed to the strong interaction between open metal sites of LnBTC and CO_2 molecules. This adsorption enthalpy is higher than those observed from MOF-508b,[60] MIL-53(Al) [61] and MOF-253,[62] but lower than those from MOFs with strong CO_2-framework interaction (such as Mg_2(dobdc) [30] and MIL-101(Cr) [63] with high polarizing adsorption sites), and amine functionalized MOFs Cu-BTTri-mmen [64] and NH_2-MIL-53(Al).[65] To some extent, the strong CO_2-framework interaction demonstrates good affinity between CO_2 molecules and the pores of MOFs, and this may be the reason of the moderate CO_2 adsorption capacity by LOFs compared with some above-mentioned MOFs.

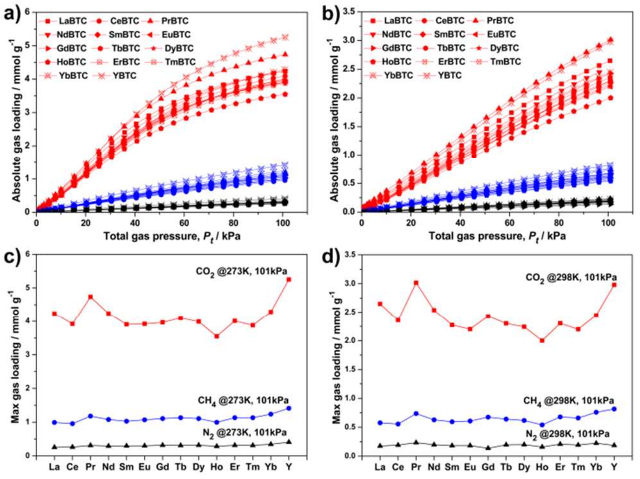

Fig. 7 CO_2, CH_4, and N_2 sorption isotherms of LnBTC at (a) 273K and (b) 298K. Red: CO_2, blue: CH_4, and black: N_2. Relationship of CO_2 uptakes and lanthanide ions in atmosphere pressure at (c) 273K and (d) 298K.

In order to observe the relationship among the lanthanide ionic radius, BET surface area and CO_2 adsorption capacity, we plot the three parameters in a three-dimensional (3D) diagram (Fig. 8). At 273 K, the highest adsorption capacity for CO_2 is YBTC, which has the highest BET surface area, lightest molecular mass, and relative small metal ionic radius among all LnBTC (Fig. 8a). For the other LnBTC, their CO_2 uptakes are proportional to the BET surface area, indicating the typical physical adsorption. Interestingly, with the temperature increasing to 298K, the highest adsorption capacity for CO_2 is PrBTC, which has still a closed proportional relationship with their BET surface area (Fig. 8b). However, the reduced CO_2 uptakes for each LnBTC from 298 K to 273 K are quite different, which should be attributed to the different intermolecular interactions of CO_2 with various open metal sites.

3.4 CO_2 separation

These LOFs exhibit much higher adsorption capacities for CO_2 than for CH_4 and N_2. Therefore may act as the potential candidates for CO_2 separation from flue gas or natural gas. CO_2 adsorption selectivities of these LOFs are calculated using ideal adsorbed solution theory (IAST)[66] based on the static saturated adsorption isotherms at 273 K and 298 K. The results are shown in Figs. S19-S32. The CO_2 adsorption isotherms of all LnBTC are fitted with the Dual-site Langmuir-Freundlich isotherm model:

$$q_i = q_{i,A,sat}\frac{b_{i,A}p_i^{v_{i,A}}}{1+b_{i,A}p_i^{v_{i,A}}} + q_{i,B,sat}\frac{b_{i,B}p_i^{v_{i,B}}}{1+b_{i,B}p_i^{v_{i,B}}}$$

Where $q_{i,sat}$ is the saturation capacity of the adsorbate *i*; b_i is Langmuir-Freundlich parameters of *i* and v_i is the exponents for the two sites A and B. All parameters are provided in Table S3-S16. For adsorption of CH_4 and N_2 in all LOFs, a single-site Langmuir model is sufficiently good for fitting purposes:

$$q_i = q_{i,sat}\frac{k_i p_i}{1+k_i p_i}$$

Where $q_{i,sat}$ is the saturation capacity of the adsorbate *i*, p_i is the partial pressure of *i*, and k_i is the adsorption constant of *i*.

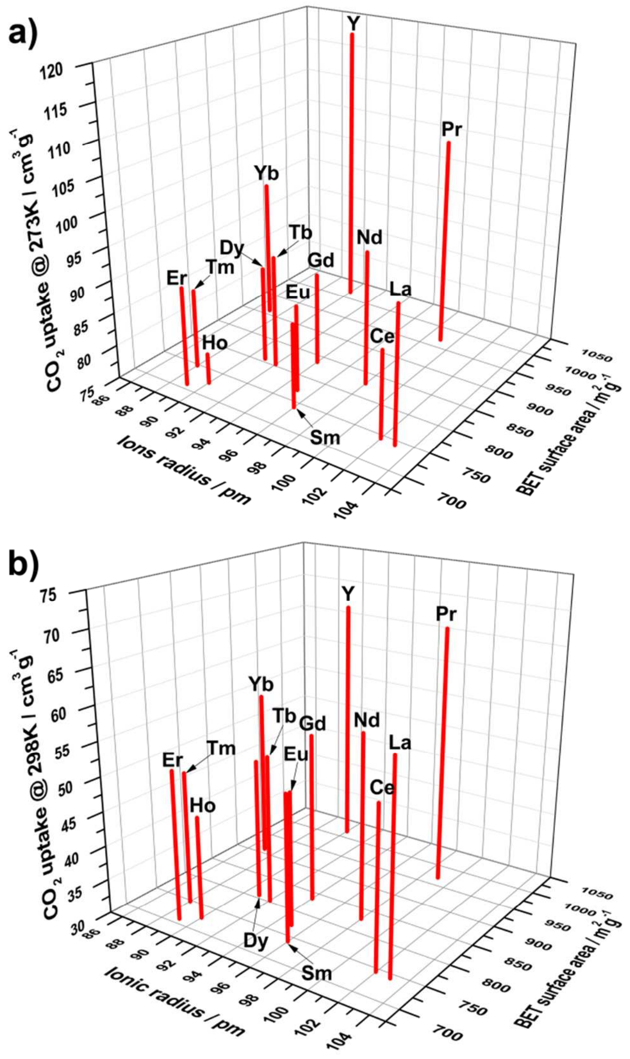

Fig. 8 Relationship of CO_2 uptakes, BET surface area, and ionic radii of Ln(III) at (a) 273K and (b) 298 K.

The Langmuir parameters of CH_4 and N_2 for LnBTC are specified in Table S17. The volumetric ratios of 1:1 for CO_2/N_2 and CO_2/CH_4 are used to predict the selectivities of binary mixtures by IAST with the partial pressure of each component of 0.2 atm, respectively. As shown in Table 1, all LnBTC exhibit high CO_2 selectivities over N_2 and CH_4 ranging from 15.8 to 29 at 273 K and 7.5 to 19.8 at 298 K for CO_2/N_2, and 3.8 to 6.2 at 273 K and 2.8 to 5.0 at 298 K for CO_2/CH_4. Their separation coefficients decrease with the decrease of ionic radii of Ln(III) induced by lanthanide contraction. LaBTC shows the highest values for both CO_2/N_2 and CO_2/CH_4. In general, increased separation coefficients are inherent important for efficient mixed gas separation while not at the expense of their adsorption amounts. In order to observe the relationship among the lanthanide ionic radius, CO_2 uptakes and CO_2 selectivities, three parameters in a 3D diagram are plotted and shown in Fig. 9. It is interesting that several LOFs with relative high CO_2 uptakes and large ionic radii exhibit higher separation coefficients than others, such as La-, Ce-, Pr-, and NdBTC. Notedly, the lanthanide contraction effects act as the vital important role to adjust their CO_2 separation capacities.

Table 1 The adsorption uptake of CO_2, CH_4 and N_2, and the selectivity calculated by IAST of LnBTC at 273 K and298 K, respectively. The partial pressures of CO_2, N_2 and CH_4 are 0.2 atm, respectively.

		Uptake (mmol/g)			Selectivity	
	Temperature	CO_2	CH_4	N_2	S_{CO_2/N_2}	S_{CO_2/CH_4}
LaBTC	273K	4.2344	0.9918	0.2556	29	6.19
	298K	2.6488	0.5766	0.1743	19.79	4.99
CeBTC	273K	3.9179	0.9561	0.2617	24.64	5.65
	298K	2.3578	0.5553	0.1906	13.03	4.04
PrBTC	273K	4.7359	1.1803	0.3106	28.48	5.87
	298K	3.0154	0.7369	0.2332	15.74	4.62
NdBTC	273K	4.2373	1.0791	0.2917	22.66	5.26
	298K	2.5385	0.6285	0.1973	13.68	3.99
SmBTC	273K	3.9020	1.0281	0.2963	21.76	5.4
	298K	2.2729	0.5947	0.1815	14.58	4.03
EuBTC	273K	3.9183	1.0696	0.2993	19.47	4.92
	298K	2.2012	0.6072	0.1823	13.32	3.66
GdBTC	273K	3.9633	1.1073	0.3177	16.96	4.39
	298K	2.4288	0.6748	0.1363	18	3.18
TbBTC	273K	4.0952	1.1329	0.3103	18.58	4.35
	298K	2.2997	0.6405	0.1964	12.21	3.42
DyBTC	273K	3.9863	1.1069	0.3174	17.42	4.31
	298K	2.2414	0.6174	0.1993	11.47	3.31
HoBTC	273K	3.5477	0.9961	0.2843	18.4	4.59
	298K	2.0019	0.5402	0.1584	15.03	3.91
ErBTC	273K	4.0065	1.1325	0.3148	16.12	4.05
	298K	2.3019	0.6792	0.2068	7.51	3.25
TmBTC	273K	3.8753	1.1318	0.3122	18.1	4.17
	298K	2.1993	0.6598	0.1930	10.8	2.88
YbBTC	273K	4.2860	1.2381	0.3444	15.85	3.84
	298K	2.4466	0.7591	0.2234	11.09	3.02
YBTC	273K	5.2544	1.4123	0.4081	17.39	4.27
	298K	2.9803	0.8163	0.1865	18.67	3.74

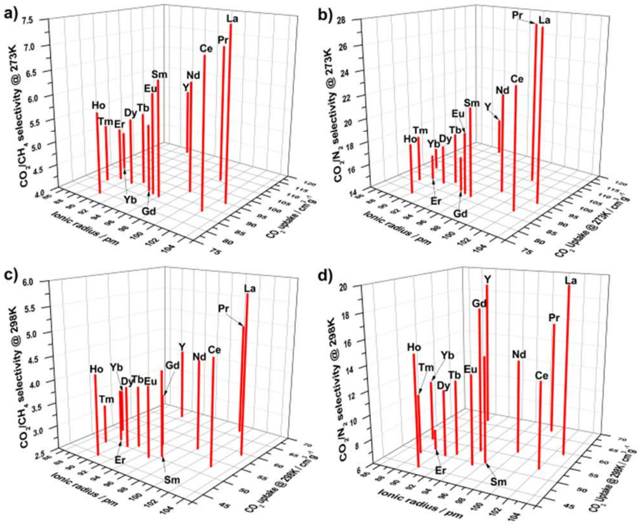

Fig. 9 Relationship of lanthanide ion radii, CO$_2$ max uptakes at 1 atm, and the simulated CO$_2$ selectivities from sorption isotherms: (a) CO$_2$/CH$_4$ in the volumetric ratios of 1:1 at 273 K, (b) CO$_2$/N$_2$ in the volumetric ratios of 1:1 at 273 K, (c) CO$_2$/CH$_4$ in the volumetric ratios of 1:1 at 298 K, and (d) CO$_2$/N$_2$ in the volumetric ratios of 1:1 at 298K.

Using He gas as the carrier gas, the real gas separations of CO$_2$ are carried out by breakthrough experiments under atmosphere pressure at 273 K and 298 K, respectively. The sample mass is listed in Table S18 for each LnBTC (Supporting Information). The mixture gases consist of 20.12% CO$_2$, 20.04% CH$_4$ and 59.86% He for CO$_2$/CH$_4$, and 20.00% CO$_2$, 20.10% N$_2$ and 59.90% He for CO$_2$/N$_2$. The CO$_2$ uptakes and selectivity from CO$_2$/CH$_4$ and CO$_2$/N$_2$ are evaluated on the basis of breakthrough curves:[67-69]

$$n_k = \frac{(\int_0^t u_i y_{k,i} dt - \int_0^t u_e y_{k,e} dt) AC - \varepsilon A L y_{k,i} p / RT}{m}$$

The composition of inlet gas is constant, but the outlet gas composition is a function of time for a definite period and the breakthrough curve is thus formed. The result of integration is provided by the mass spectrograph. The separation coefficient of adsorption is defined as:[70]

$$Selectivity = \frac{n_j}{n_i} \times \frac{x_i}{x_j}$$

Where x and y is the molar fraction of components i and j in the adsorbed phase and the gas phase at equilibrium, respectively. All breakthrough curves are summarized in Figs. S33 to S46.

As shown in Fig. 10, the highest CO$_2$ separation coefficients for CO$_2$/CH$_4$ happen to be SmBTC (5.72 at 273K) and LaBTC (5.55 at 298K), respectively. Interestingly, YBTC with high CO$_2$ uptake exhibits a quite low CO$_2$ selectivities (2.775 at 273 K and 2.15 at 298K) versus CH$_4$ although it has the lightest molecular mass and highest BET surface area, which is close to the lowest ones as HoBTC (2.21) at 273 K and YbBTC (2.09) at 298 K (Fig. 10a,c). This result indicates the open metal sites within LnBTC have weak interaction with CH$_4$ in the gas mixtures and result in relative low selectivities to CO$_2$. However, for CO$_2$/N$_2$ dynamic separation, the phenomena are quite different from that of CO$_2$/CH$_4$. The highest CO$_2$ separation coefficients are observed for LaBTC (14.56 at 273K) and HoBTC (10.88 at 298K), respectively (Fig. 10b,d). Instead, YBTC also exhibits a quite high CO$_2$ selectivities (9.27 at 273 K and 9.71 at 298K) versus N$_2$, implying YBTC has a much weaker interactions with N$_2$ than CO$_2$ at these conditions. It is worthwhile to note that the overall dynamic CO$_2$ selectivities for both CO$_2$/CH$_4$ and CO$_2$/N$_4$ are lower than those of simulated from static saturated adsorption experiments at a similar pressure and temperature conditions. This may be attributed to the synergetic effect in real gas mixtures.[71]

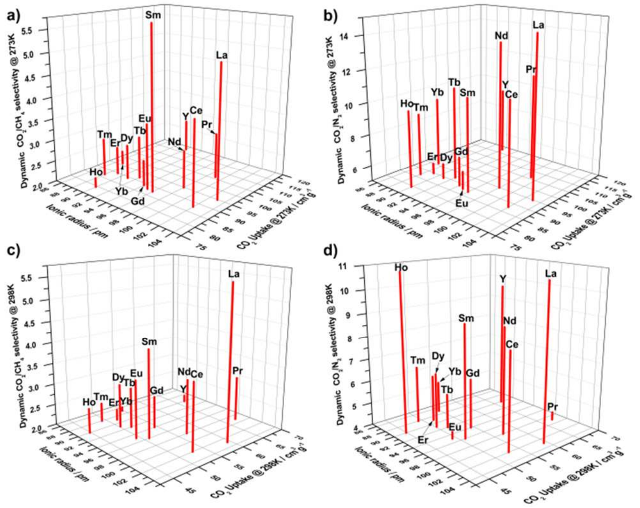

Fig. 10 Relationship of lanthanide ion radii, CO$_2$ max uptakes at 1 atm, CO$_2$ selectivities from real gas mixtures: (a) CO$_2$/CH$_4$ at 273 K, (b) CO$_2$/N$_2$ at 273 K, (c) CO$_2$/CH$_4$ at 298 K, and (d) CO$_2$/N$_2$ at 298K.

4. Conclusions

In summary, a family of porous LOF materials with microporous structures and open metal sites are facilely prepared and easily scaled in a remarkably short time. These LOFs exhibit excellent high thermal stabilities and permanent porosity even after removal of coordinating solvent molecules. More interestingly, lanthanide contraction remarkably affects their performances for CO$_2$ capture and separation. The results from this investigation suggest that the thermostable porous LOFs is promising for their application in carbon dioxide capture from flue gas and natural gas to reduce the greenhouse emissions and improve energy efficiency.

Acknowledgements

We acknowledge that financial support from National Natural Science Foundation of China 11175006, 51322205 and 21371014, the Ministry of education program for New Century Excellent Talents of China (NCET-11-0027), and Singapore-Peking University SPURc program.

Notes and References

[1] *Department of Materials Science and Engineering, College of Engineering, Peking University, Beijing 100871, China. Fax: +86-10-82529010; Tel: +86-10-82529045; E-mail: rzou@pku.edu.cn.*
[2] *State Key Laboratory of Heavy Oil Processing, China University of Petroleum, Beijing, 102249, China*

†Electronic Supplementary Information (ESI) available: ISI stastical result about photographs of synthesized LnBTC (Fig. S1), PXRD patterns of YBTC after the reaction of 1 h and 17 h, respectively (Fig. S2), comparison of TGA curves of as-synthesized YBTC sample and activated sample (Fig. S3), pure component isotherm data for CO$_2$, CH$_4$ and N$_2$ in LnBTC (Fig. S4-S17), isosteric heat of LnBTC (Fig. S18), adsorption selectivity calculated by IAST (Fig. S19-S32), breakthrough curves of LnBTC (Fig. S33-S46), ionic radii of Ln(III) (Table S1), pore parameters of as synthesized LOFs (Table S2), adsorption model parameters in LnBTC (Table S3-S17) and sample mass of the activated LnBTC for breakthrough experiments (Table S18). For ESI or other electronic format see DOI: 10.1039/b000000x/.

1 IPCC, 2007: Climate Change 2007: Synthesis Report. *IPCC*, Geneva, Switzerland, 2007.

2 D. P. Schrag, *Science*, 2007, **5813**, 812-813.

3 K. T. Chue, J. N. Kim, Y. J. Yoo, S. H. Cho and R. T. Yang, *Ind. Eng. Chem. Res.*, 1995, **34**, 591-598.

4 R. Kumar, *Ind. Eng. Chem. Res.*, 1994, **33**, 1600-1605.

5 M. T. Ho, G. W. Allinson and D. E. Wiley, *Ind. Eng. Chem. Res.*, 2008, **47**, 4883-4890.

6 S. R. Batten, N. R. Champness, X. M. Chen, J. Garcia-Martinez, S. Kitagawa, L. Öhrström, M. O'Keeffe, M. P. Suh and J. Reedijk, *Pure Appl. Chem.*, 2013, **85**, 1715-1724.

7 R. Babarao, Z. Hu, J. Jiang, S. Chempath and S. I. Sandler, *Langmuir*, 2007, **23**, 659-666.

8 D. Britt, H. Furukawa, B. Wang, T. G. Glover and O. M. Yaghi, *P. Natl. Acad. Sci. USA*, 2009, **106**, 20637-20640.

9 P. Nugent, Y. Belmabkhout, S. D. Burd, A. J. Cairns, R. Luebke, K. Forrest, T. Pham, S. Ma, B. Space, L. Wojtas, M. Eddaoudi and M. J. Zaworotko, *Nature*, 2013, **495**, 80-84.

10 J. Liu, J. Tian, P. K. Thallapally and B. P. McGrail, *J. Phys. Chem. C*, 2012, **116**, 9575-9581.

11 J. An, S. J. Geib and N. L. Rosi, *J. Am. Chem. Soc.*, 2009, **132**, 38-39.

12 B. Liu, L. X. Tang, Y. H. Lian, Z. Li, C. Y. Sun and G. J. Chen, *Acta Chim. Sinica*, 2013, **71**, 920-928.

13 S. Vaesen, V. Guillerm, Q. Y. Yang, A. D. Wiersum, B. Marszalek, B. Gil, A. Vimont, M. Daturi, T. Devic, P. L. Llewellyn, C. Serre, G. Maurin and G. De Weireld, *Chem. Commun.*, 2013, **49**, 10082-10084.

14 I. Spanopoulos, P. Xydias, C. D. Malliakas and P. N. Trikalitis, *Inorg. Chem.*, 2013, **52**, 855-862.

15 P. Z. Li and Y. L. Zhao, *Chem. Asian J.*, 2013, **8**, 1680-1691.

16 D.-X. Xue, A. J. Cairns, Y. Belmabkhout, L. Wojtas, Y. Liu, M. H. Alkordi and M. Eddaoudi, *J. Am. Chem. Soc.*, 2013, **135**, 7660-7667.

17 Q. J. Yan, Y. C. Lin, P. Y. Wu, L. Zhao, L. J. Cao, L. M. Peng, C. L. Kong and L. Chen, *Chempluschem*, 2013, **78**, 86-91.

18 H. Xu, Y. B. He, Z. J. Zhang, S. C. Xiang, J. F. Cai, Y. J. Cui, Y. Yang, G. D. Qian and B. L. Chen, *J. Mater. Chem. A*, 2013, **1**, 77-81.

19 Z. Bao, L. Yu, Q. Ren, X. Lu and S. Deng, *J. Colloid Interface Sci.*, 2011, **353**, 549-556.

20 A. Demessence, D. M. D'Alessandro, M. L. Foo and J. R. Long, *J. Am. Chem. Soc.*, 2009, **131**, 8784-8786.

21 J. L. C. Rowsell, A. R. Millward, K. S. Park and O. M. Yaghi, *J. Am. Chem. Soc.*, 2004, **126**, 5666-5667.

22 T. M. McDonald, W. R. Lee, J. A. Mason, B. M. Wiers, C. S. Hong and J. R. Long, *J. Am. Chem. Soc.*, 2012, **134**, 7056-7065.

23 Z. J. Zhang, W. Y. Gao, L. Wojtas, S. Q. Ma, M. Eddaoudi and M. J. Zaworotko, *Angew. Chem. Int. Ed.*, 2012, **51**, 9330-9334.

24 B. Zornoza, A. Martinez-Joaristi, P. Serra-Crespo, C. Tellez, J. Coronas, J. Gascon and F. Kapteijn, *Chem. Commun.*, 2011, **47**, 9522-9524.

25 A. K. Chaudhari, S. Mukherjee, S. S. Nagarkar, B. Joarder and S. K. Ghosh, *CrystEngComm*, 2013, **15**, 9465-9471.

26 P. He, H. Liu, Y. F. Li, Z. G. Lei, S. P. Huang, P. Wang and H. P. Tian, *Mol. Simulat.*, 2012, **38**, 72-83.

27 T. Li and N. L. Rosi, *Chem. Commun.*, 2013, **49**, 11385-11387.

28 R. Babarao, M. Eddaoudi and J. W. Jiang, *Langmuir*, 2010, **26**, 11196-11203.

29 J. B. Decoste, G. W. Peterson, M. W. Smith, C. A. Stone and C. R. Willis, *J. Am. Chem. Soc.*, 2012, **134**, 1486-1489.

30 S. R. Caskey, A. G. Wong-Foy and A. J. Matzger, J. Am. Chem. Soc., 2008, **130**, 10870-10871.

31 Z. Lin, R. Zou, W. Xia, L. Chen, X. Wang, F. Liao, Y. Wang, J. Lin and A. K. Burrell, *J. Mater. Chem.*, 2012, **22**, 21076-21084.

32 L. Yan, Q. Yue, Q. X. Jia, G. Lemercier and E. Q. Gao, Cryst. *Growth Des.*, 2009, **9**, 2984-2987.

33 J. Rocha, L. D. Carlos, F. A. A. Paz and D. Ananias, *Chem. Soc. Rev.*, 2011, **40**, 926-940.

34 Z. Li, G. Zhu, X. Guo, X. Zhao, Z. Jin and S. Qiu, *Inorg. Chem.*, 2007, **46**, 5174-5178.

35 F. Gándara, A. D. Andrés, B. Gómez-Lor, E. Gutiérrez-Puebla, M. Iglesias, M. A. Monge, D. M. Proserpio and N. Snejko, *Cryst. Growth Des.*, 2008, **8**, 378-380.

36 J. M. Zhou, W. Shi, N. Xu and P. Cheng, *Inorg. Chem.*, 2013, **52**, 8082-8090.

37 O. Guillou and C. Daiguebonne, Handbook on the Physics and Chemistry of Rare Earths. Elsevier, New York , 2005, 359-404.

38 S. Ganguly, P. Pachfule, S. Bala, A. Goswami, S. Bhattacharya and R. Mondal, *Inorg. Chem.*, 2013, **52**, 3588-3590.

39 H. L. Jiang, N. Tsumori and Q. Xu, *Inorg. Chem.*, 2010, **49**, 10001-10006.

40 L. H. Xie, Y. Wang, X. M. Liu, J.B. Lin, J. P. Zhang and X. M. Chen, *CrystEngComm*, 2011, **13**, 5849-5857.

41 K. Tang, R. Yun, Z. Lu, L. Du, M. Zhang, Q. Wang and H. Liu, *Cryst. Growth Des.*, 2013, **13**, 1382-1385.

42 Z. Lin, R. Zou, J. Liang, W. Xia, D. Xia, Y. Wang, J. Lin, T. Hu, Q. Chen, X. Wang, Y. Zhao and A. K. Burrell, *J. Mater. Chem.*, 2012, **22**, 7813-7818.

43 B. Mu, F. Li, Y. Huang and K. S. Walton, *J. Physical. Chem.*, 2012, **22**, 10172-10178.

44 T. K. Maji, G. Mostafa, H. C. Chang and S. Kitagawa, *Chem. Commun.*, 2005, **19**, 2436-2438.

45 Y. Q. Lan, H. L. Jiang, S. L. Li and Q. Xu, *Adv. Mater.*, 2011, **23**, 5015-5020.

46 X. Guo, G. Zhu, Z. Li, F. Sun, Z. Yang and S. Qiu, *Chem. Commun.*, 2006, **30**, 3172-3174.

47 N. A. Khan, M. M, Haque and S. H. Jhung, *Eur. J. Inorg. Chem.*, 2010, **31**, 4975-4981.

48 T. Devic, C. Serre, N. Audebrand, J. Marrot and G. Férey, *J. Am. Chem. Soc.*, 2005, **127**, 12788-12789.

49 H. He, H. Ma, D. Sun, L. Zhang, R. Wang and D. Sun, *Cryst. Growth Des.*, 2013, **13**, 3154-3161.

50 J. Luo, H. Xu, Y. Liu, Y. Zhao, L. L. Daemen, C. Brown, T. V. Timofeeva, S. Ma and H. C. Zhou, *J. Am. Chem. Soc.*, 2008, **130**, 9626-9627.

51 S. Mohapatra, K. P. S. S. Hembram, U. Waghmare and T. K. Maji, *Chem. Mater.*, 2009, **21**, 5406-5412.

52 Y. He, H. Furukawa, C. Wu, M. O'Keeffe, R. Krishna and B. Chen, *Chem. Commun.*, 2013, **49**, 6773-6775.

53 M. Gustafsson, A. Bartoszewicz, B. Martín-Matute, J. Sun, J. Grins, T. Zhao, Z. Li, G. Zhu and X. Zou, *Chem. Mater.*, 2010, **22**, 3316-3322.

54 Topas V2.1: General Profile and Structure Analysis Software for Powder Diffraction data, Bruker AXS, Karlsruhe, Germany, 2002.

55 R. Zou, R. Zhong, M. Du, T. Kiyobayashi and Q. Xu, *Chem. Commun.*, 2007, **24**, 2467-2469.

56 S. Ma, X. S. Wang, D. Yuan and H. C. Zhou, *Angew. Chem. Int. Ed.*, 2008, **47**, 4130-4133.

57 Y. Li, Z. Ju, B. Wu and D. Yuan, *Cryst. Growth Des.*, 2013, **13**, 4125-4130.

58 T. W. Kim, I. Y. Kim, T. S. Jung, C. H. Ko and S. J. Hwang, *Adv. Funct. Mater.*, 2013, **35**, 4377-4385.

59 H. Pan, J. A. Ritter and P. B. Balbuena, *Langmuir*, 1998, **14**, 6323-6327.

60 L. Bastin, P. S. Barcia, E. J. Hurtado, J. A. Silva, A. E. Rodrigues and B. Chen, *J. Phys. Chem. C.*, 2008, **112**, 1575-1581.

61 D. W. Keith, M. Ha-Duong and J. K. Stolaroff, *Climatic Change*, 2006, **74**, 17-45.

62 P. K. Thallapally, J. Tian, M. R. Kishan, C. A. Fernandez, S. J. Dalgarno, P. B. McGrail, J. E. Warren and J. L. Atwood, *J. Am. Chem. Soc.*, 2008, **130**, 16842-16843.

63 P. L. Llewellyn, S. Bourrelly, C. Serre, A. Vimont, M. Daturi, L. Hamon, G. D. Weireld, J.-S. Chang, D.-Y. Hong, Y. K. Hwang, S. H. Jhung and G. Férey, *Langmuir*, 2008, **24**, 7245-7250.

64 T. M. McDonald, D. M. D'Alessandro, R. Krishna and J. R. Long, *Chem. Sci.*, 2011, **2**, 2022-2028.

65 B. Arstad, H. Fjellvåg, K. O. Kongshaug, O. Swang and R. Blom, *Adsorption*, 2008, **14**, 755-762.

66 A. L. Myers and J. M. Prausnitz, *AIChE Journal*, 1965, **11**, 121-127.

67 A. Malek, S. Farooq, M. N. Rathor and K. Hidajat, *Chem. Eng. Sci.*, 1995, **50**, 737-740.

68 X. Liu, J. Li, L. Zhou, D. Huang and Y. Zhou, *Chem. Phys. Lett.*, 2005, **415**, 198-201.

69 X. Liu, L. Zhou, X. Fu, Y. Sun, W. Su, Y. Zhou, *Chem. Eng. Sci.*, 2007, **62**, 1101-1110.

70 D. M. Ruthven, Principles of adsorption and adsorption processes, John Wiley & Sons, 1984.

71 H. Sato, W. Kosaka, R. Matsuda, A. Hori, Y. Hijikata, R. V. Belosludov, S. Sakaki, M. Takata and S. Kitagawa, *Science*, 2014, **343**, 167-170.